Submitted to Nucl. Phys. B, Dec. 1978

Inclusive and Semi-inclusive Charge Structure in $\pi^- p$ Multiparticle Production at 147 GeV/c*

D. Brick, A. M. Shapiro, M. Widgoff
Brown University, Providence, Rhode Island 02912

F. Barreiro§, O. Benary†, J. E. Brau‡, E. S. Hafen, R. I. Hulsizer, V. Kistiakowsky, A. Napier, S. H. Oh, I. A. Pless, J. P. Silverman, P. C. Trepagnier, R. K. Yamamoto
Laboratory for Nuclear Science and Department of Physics
Massachusetts Institute of Technology, Cambridge, Massachusetts 02139

W. Kittel, M. Schouten
Nijmegen University, Nijmegen, The Netherlands

H. O. Cohn
Oak Ridge National Laboratory, Oak Ridge, Tennessee 37830

P. Jacques, P. Stamer, T. L. Watts
Rutgers University, New Brunswick, New Jersey 08854

E. B. Brucker, E. L. Koller
Stevens Institute of Technology, Hoboken, New Jersey 07030

W. M. Bugg, T. Handler
University of Tennessee, Knoxville, Tennessee 37916

Abstract

A new method of analysis (Leading Charge Model) based on the zone graph technique is used to separate charged particles produced in the target, projectile, and central regions of phase space. A significant fraction of the centrally produced particles follow a Bose momentum distribution with temperature of 131 ± 2 MeV.

---

* This work is supported in part by the U. S. Department of Energy and the National Science Foundation.

§ Present address: DESY, Hamburg, West Germany.

† Permanent address: Tel-Aviv University.

‡ Present address: SLAC, Stanford, California.

Introduction

Many experiments have now produced evidence supporting local compensation of charge in hadronic reactions. One example of such evidence appears in the zone graph analysis of charge structure in pp interactions at 102 GeV/c and 400 GeV/c[1] and in π^-p interactions at 200 GeV/c.[2] At the same time, fragmentation-like processes exhibit a strong influence on the charge structure of these reactions (2a, 2b, 2c). In this work we present the zone graph properties of 147 GeV/c π^-p events in the Fermilab 30-inch Proportional Wire Hybrid Spectrometer. We compare these properties with a random charge model and a strongly ordered charge model. The data deviate strongly from both and display a charge structure that is well expressed by a leading charge model in which particle production comes from three sources: beam fragmentation, target fragmentation, and central production. After comparing the zone graph features with these three models, we examine the rapidity gap distributions and find that they also exhibit charge structure which is consistent with the leading charge model. Finally, the properties of the central production isolated by the leading charge model are presented.

Our data come from a 105,000 picture exposure in the Fermilab 30-inch Hybrid Spectrometer which is described in detail elsewhere.[3] The downstream proportional wire chambers give a momentum resolution ($\Delta p/p$) for fast secondaries of 0.06% p (GeV/c). The film was first measured on the M. I. T. PEPR system. Failed and incomplete events were examined and remeasured on manual machines, resulting in a data sample of about 6866 complete events. Protons with momenta less than 1.4 GeV/c were identified by ionization and all other secondaries were assigned pion masses. Elastic events were removed by using the measurement of the recoil proton in the bubble chamber to predict the trajectory of the outgoing fast pion under the hypothesis that the event was elastic and then comparing the prediction with the observed trajectory in the downstream electronic chambers (see ref. [3]).

Zone Graph Analysis

The zone graph technique formulated by Krzywicki and Weingarten[4] assigns the particles in rapidity space to neutral charge zones. For an event with N charged particles, the zone graph function, $Z(y)$, is given by

$$Z(y) = \sum_{i=1}^{N} q_i \, \epsilon (y-y_i) - q_{beam} \, \epsilon (y-y_{beam}) - q_{target} \, \epsilon (y-y_{target})$$

where q_i is the charge of particle i and $\epsilon (y-y_i)$ is the usual step function which is 1 for $y \geq y_i$ and 0 otherwise. Figure 1 illustrates the construction of a zone graph for a ten prong event. Regions of rapidity over which $Z(y)$ remains nonzero are called zones; gaps where $Z(y) = 0$ separate each successive pair of zones. Zones containing either beam or target particles are called end zones and zones containing only final state particles are called central zones. Notice that $-Z(y)$ is the charge transferred across the rapidity y so that the usual charge transfer variable,[5] u, is equal to $-Z(0)$.

The zone graph properties, such as number of zones per event, number of particles per zone, rapidity intervals between ends of zones, or rapidity distribution of zone centers, quantify the charge structure of the data. For reference, it is useful to compare this structure with models representing two extremes of charge structure: a non-ordered model in which no structure is imposed, and a strongly ordered model in which maximal charge structure appears. The random charge model (RCM) comparison is carried out using events created by randomly reassigning the charges of the measured particles. The other extreme, which we will refer to as the extreme compensation model (ECM), is created by reassigning charges to the data in a strictly ordered fashion. The first particle in rapidity is assigned the charge of the target (positive), the last particle in rapidity is assigned the charge of the beam (negative), and the other particles are grouped into adjacent positive-negative pairs. This model represents in some approximation the strongly-ordered multiperipheral model.

While these two models represent the extremes of charge structure, we find that the data contain significantly more structure than the random charge model and significantly less structure than the extreme compensation model. We compare the data with an intermediate case which we call the leading charge model (LCM), which assumes charge structure resulting from leading charge effects along with a structureless central region. This model, too, is tested by reassigning charges of the data. First the leading clusters (forward-going and backward-going) are identified. Then the charges of the leading clusters are held fixed while the charges of the central particles are randomly reassigned. The leading clusters are defined as the end zones in the zone graphs with the addition of positive-negative charge pairs which are near to the end zones in rapidity space.* Particles not in a leading cluster are defined to be in the central region.

Figure 2 displays the charge transfer ($u = -Z(0)$) distribution for our 147 GeV/c $\pi^- p$ data. Also shown on figure 2 are the results of applying the random charge model and the leading charge model to the data. The random charge model represents an extreme bound for the data while the leading charge model appears to express its major features. Table I presents the dispersion ($\langle u^2 \rangle - \langle u \rangle^2$) of the charge transfer for the data and the models. The data contains slightly more local compensation of charge than the leading charge model.

The first measure of zone structure comes from the distribution of the number of zones per event. As figure 3 shows, the data rarely contain a single zone. The random charge model results in events with relatively few zones, while the extreme compensation model results in many zones. The leading charge model reproduces the principal features of the data.

---

* This addition accounts for the situation in which a multiple-particle cluster distributes itself in rapidity in such a way that some particles are left out of the end zone. For example, a three particle leading cluster (assuming a random break-up) will result in a single particle falling in the end zone two thirds of the time. Rapidity cuts were used to add the positive-negative pairs such that the defined three-body leading clusters had a single particle end zone two thirds of the time.

The semi-inclusive distributions for the number of zones per event are shown in figure 4. Here, as in the inclusive distribution, the leading charge model (LCM) reproduces the data reasonably well. Table II presents the semi-inclusive average number of zones per event and compares these with the values obtained from the three models. The multiplicity dependence exhibited by the data follows that of the leading charge model.

The average multiplicity of central zones is summarized in Table III. The average multiplicities increase with the charge multiplicity of the event. The data generally fall between the extreme compensation model and the random charge model, as does the leading charge model. Figure 5 presents the distribution of central zone lengths. The random charge model differs from the data principally in normalization since in the random charge model many more particles appear in end zones. The extreme compensation model has many more short central zones and fewer long central zones than the data. The leading charge model is the most successful of the three in reproducing the data. Table IV presents the data for the average central zone lengths and the model values.

The rapidity distribution of particles in the central zones is shown in figure 6. The leading charge model, with random charge assignments among the central particles, apparently has the proper amount of local compensation of charge since it reproduces this distribution.

Rapidity Gaps and Associated Charge-Exchange

The charge exchanged across rapidity gaps as a function of the gap length is another measure of charge structure. Each rapidity gap is labeled by its length and by the amount of charge transferred across it. First the n-charged particles are ordered in rapidity so that $y_1 < y_2 \ldots\ldots < y_n$. Then, the ith rapidity gap has length

$$\Delta y_i = y_{i+1} - y_i$$

and carries charge

$$\Delta Q_i = \left(\sum_{j=1}^{i} q_j\right) - q_t$$

where q_j is the charge of the jth particle and q_t is the charge of the target. Note that odd-numbered gaps always carry even charge and even-numbered gaps always carry odd charge.

Previous authors[6, 7] have noted the absence of large rapidity gaps with more than one unit of charge exchanged. Figure 7 shows the distributions of rapidity gaps carrying charge 0, $\pm$ 1, or $\pm$ 2. End gaps have been removed from these distributions. The number of gaps carrying charge $\pm$ 2 falls more rapidly with gap length than does the number carrying charge 0 or $\pm$ 1. This effect has been interpreted as evidence that the exchanges in multiparticle production carry charges 0 or $\pm$ 1 while the charge exchange $\pm$ 2 gaps come from crossovers of particles along a multiperipheral chain. Crossovers would be expected mainly for small rapidity gaps just where the charge exchange $\pm$ 2 gaps occur most.

One can define the probability ($P_{\Delta Q}(\Delta y)$) for finding a specific value of charge exchange for a given gap length.[7] This probability is normalized separately for even and odd gaps so that

$$\sum_{\Delta Q_{even}} P_{\Delta Q}(\Delta y) = 1$$

$$\sum_{\Delta Q_{odd}} P_{\Delta Q}(\Delta y) = 1 \ .$$

Figure 8 shows $P_{\Delta Q = \pm 2}(\Delta y)$ distributions. The probability of observing a gap with a charge exchange of $\pm$ 2 decreases with the gap length. The probability function $P_{\Delta Q = \pm 2}(\Delta y)$ is compared with the random charge model and the leading charge model. The extreme compensation model cannot produce gaps with charges of $\pm$ 2.

The random charge model has a probability near one-half and approximately independent of the gap length, while the probability distribution of the leading charge model preserves the fall off with gap length for exchange of ± 2 units of charge. This effect is examined semi-inclusively by defining two variables which summarize the charge exchanges across rapidity gaps. The first is just the event-to-event average of the sum of the absolute value of all exchanges in the event:[8]

$$V_1 = \sum_{i=1}^{n-1} |\Delta Q_i| .$$

A second variable, which weights large gaps more than small gaps, is

$$V_2 = \frac{\sum_{i=1}^{n-1} |\Delta Q_i| \Delta y_i}{\sum_{i=1}^{n-1} \Delta y_i} .$$

Figure 9 presents the measurements of V_1 compared to the values given by the three models. The data clearly show for all multiplicities an absence of gaps carrying a large amount of charge, unlike the random charge model, whereas the leading charge model agrees very well with the data.

Figure 10 presents the measurements and model values of V_2. Again, the absence of gaps with large amounts of charge is clear for all multiplicities. The leading charge model reproduces the data well.

Central Production

The preceding sections have demonstrated that the leading charge model reproduces the principal charge structure of the data. This model implies that the pion-proton multiparticle production reactions of this experiment may develop through a production mechanism in which two leading particles (or clusters) are produced in association with a central fireball. *

* The name "fireball" was introduced by G. Cocconi[9] in reference to an object which decays into pions isotropically. We shall see that a large fraction of the products of our central region behave as though they have been produced isotropically in some rest frame.

We will now turn our attention to studying the properties of the isolated central production. The leading charge model assumes that the charges of the pions in the central region are random. This means that the π^+ and the π^- rapidity distributions must be similar. In fact, this observation is the first indication that the isolated central production may come from a fireball. An earlier investigation of inclusive rapidity distributions from this experiment showed there is no central region where the π^+ and the π^- rapidity distributions are identical.[2a] The difference between the rapidity distributions for π^+'s and that for π^-'s in π^-p interactions passes through zero near y = 0, but there is no flattening of this difference about y = 0. Figure 11a shows the asymmetry

$$A(y) = \frac{\left(\frac{d\sigma}{dy}\right)_+ - \left(\frac{d\sigma}{dy}\right)_-}{\left(\frac{d\sigma}{dy}\right)_+ + \left(\frac{d\sigma}{dy}\right)_-} \quad .$$

As figure 11a shows, the positive particles outnumber negative particles for negative rapidities and the negatives outnumber positives for positive rapidities. There is no central region where both charges appear in equal numbers. Figure 11b shows the asymmetry when only central zone particles are included. A region of about two rapidity units in extent appears where positive and negative charges exist in equal numbers.

Van Hove[10] has defined a cluster as an aggregate of final state particles such that in the rest system of this aggregate the longitudinal and the transverse momenta of the particles are similar. In figure 12a the center of mass longitudinal and transverse (along one transverse direction) momenta of all final particles in the π^-p interactions are compared. The particles clearly contain larger amounts of longitudinal momenta than transverse momenta. This feature is the well known effect of

limited transverse momenta. Figure 12b shows a comparison of the longitudinal and transverse momenta of charged particles in the central fireball. These momenta are defined in the center of mass of the charged particles in the central fireball. The two components follow very similar distributions and satisfy Van Hove's definition of a cluster.

Having shown that the momenta of charged particles in the fireball behave similarly, transverse to and along the interaction axis, we shall now investigate the angular distribution of these particles. Figure 13 shows these distributions for the $\pi^- p$ data as a function of the particle momenta in the fireball rest frame. The angle θ is the angle between the particle's momentum vector and the beam direction. The distributions of particles with momenta less than 400 MeV/c (53% of the particles) are completely isotropic. The particles with momenta in excess of 400 MeV/c (and especially those above 600 MeV/c) exhibit forward-backward peaking. It is the isotropic behavior of the low momentum particles, along with the random charge assignments, which leads us to refer to this as the central fireball.

Figure 14 shows the multiplicity distribution for the central fireball. The multiplicity as a function of the mass of the fireball can be compared with statistical theory predictions. The Fermi[11] and Landau[12] theories predict an $M^{\frac{1}{2}}$ dependence, Pomeranchuk[13] devised a linear mass dependence, and recent hydrodynamic models[14] show that the mass dependence hinges strongly on the speed of sound in nuclear matter. Feinberg[15] has included a description of viscosity estimated by quantum-field methods in the Landau model to derive an $M^{\frac{2}{3}}$ dependence. We are restricted to measuring the mass of the charged particles, but the functional dependence should be the same. The mass dependence of the average charged multiplicity is presented in figure 15. The best fit of the form

$$\langle n \rangle = M^b$$

yields $b = .70 \pm .01$ (with $\chi^2 = 2.35$ per degree of freedom).

Figure 16 displays the momentum distribution of fireball particles. The data were fit to a Bose distribution of the form

$$F(p) \frac{A\, p^2}{e^{E/T} - 1}$$

for $p < 800$ MeV/c and $E = (p^2 + M_\pi^2)^{\frac{1}{2}}$. The fit gave a temperature for the fireball of 131 ± 2 MeV (with $\chi^2 = 2.8$ per degree of freedom).

Conclusions and Discussion

This work presents the results of a study of $\pi^- p$ multiparticle production reactions at 147 GeV/c. The details of zone graphs and charge exchange across rapidity gaps are consistent with a leading charge model in which events proceed through the production of three distinct groupings in phase space: two leading particles or clusters and a central cluster. This picture of multiparticle production resembles the model of Pokorski and Van Hove[16] in which the valence quarks of the interacting hadrons pass through the interaction region retaining their internal quantum numbers and subsequently fragment into a leading cluster. In their model, central production emerges from the gluons of the interacting hadrons.

We find a large fraction of the central particles have features consistent with having come from an isotropically decaying central fireball. The secondaries from the fireball follow a Bose momentum distribution with a temperature of 131 ± 2 MeV. In terms of the maximal possible temperature ($T_0 = 160$ MeV) of the Hagedorn statistical and thermodynamical theory,[19] this temperature is $(0.82 \pm .01) T_0$.

The evidence for central fireball production found in this experiment is consistent with a multiperipheral cluster model description of particle production derived from the Bethe-Salpeter equation for the scattering amplitude.[18] This model

expects an average of one central fireball at energies around 100 GeV and an average of two at energies of about 1 TeV.[17]

We thank the PHSC[20] for the use of its 147 GeV/c π^-p data. We also thank Fermilab and its Neutrino Department for making the experiment possible and our scanning and measuring staffs for carrying out their tasks in a skillful and proficient manner. This work was supported in part by funds provided by the U. S. Department of Energy and the National Science Foundation. One of us (J. E. B.) also wishes to acknowledge the support of the Fannie and John Hertz Foundation.

References

1. C. Bromberg et al., Phys. Rev. D12 (1975) 1224.
2. V. A. Sreedhar et al., Phys. Rev. D14 (1976) 2394.

2a. D. Fong et al., Phys. Lett. 61B (1976) 99.

2b. V. P. Kenney et al., "Leading Clusters" in 200 GeV/c π^-p Inclusive Reactions, Proc. of the EPS International Conf., Palermo (1975) 815.

2c. W. B. Fretter et al., Phys. Lett. 57B (1975) 197.

3. D. Fong et al., Nucl. Phys. B102 (1976) 386;
   D. Fong et al., Phys. Lett. 53B (1974) 290.
4. A. Krzywicki and D. Weingarten, Phys. Lett. 50B (1974) 265.
5. T. T. Chou and C. N. Yang, Phys. Rev. D7 (1973) 1425.
6. P. Pirila, G. H. Thomas, and C. Quigg, Phys. Rev. D12 (1975) 92.
7. J. W. Lamsa et al., Phys. Rev. Lett. 37 (1976) 73.
8. H. Braun et al., Phys. Rev. D17 (1978) 1260.
9. G. Cocconi, Phys. Rev. 111 (1958) 1699.
10. L. Van Hove, Hadron Scattering at High Energies (Theory), Proc. of the Hawaii Topical Conf. in Particle Phys., Honolulu (1969) 115.
11. E. Fermi, Progr. Theor. Phys. 5 (1950) 570.
12. L. D. Landau, Izv. Akad. Nauk SSSR 17 (1953) 51.
13. I. Ya. Pomeranchuk, Dokl. Acad. Nauk SSSR 78 (1951) 889.
14. F. Cooper, C. Frye, and E. Schonberg, Phys. Rev. D11 (1975) 192.
15. E. L. Feinberg, Soviet Physics Uspekhi 14 (1972) 455.
16. S. Pokorski and L. Van Hove, Acta Phys. Pol B5 (1974) 229.
17. M. Miesowicz, Fireball Model of Meson Production, Progress in Elementary Particle and Cosmic Ray Physics, vol. X (1971) 103.
18. I. M. Dremin and A. M. Dunaevskii, Physics Reports 18C (1975) 159.

19. R. Hagedorn, Suppl. Il Nuovo Cimento 3 (1965) 147;
R. Hagedorn and J. Ranft, Suppl. Il Nuovo Cimento 6 (1968) 169;
R. Hagedorn, Suppl. Il Nuovo Cimento 6 (1968) 311.

20. The PHSC (Proportional Hybrid System Consortium) consists of groups from Brown University, CERN, Fermilab, Illinois Institute of Technology, University of Illinois, Indiana University, Johns Hopkins University, Massachusetts Institute of Technology, Oak Ridge National Laboratory, Rutgers University, Stevens Institute of Technology, University of Tennessee, and Yale University. See reference (2a) for author list.

Figure Captions

Figure 1: Construction of a zone graph for a hypothetical 10-prong event.

Figure 2: Charge transfer distribution with predictions of the random charge model (RCM) and leading charge model (LCM).

Figure 3: Zone multiplicity distributions showing the probability for obtaining various numbers of zones from the data and the (RCM), (ECM), and (LCM) models.

Figure 4: Semi-inclusive zone distributions depicting cross section versus number of zones for the various prong multiplicities, along with the results of the (RCM) and (LCM) models.

Figure 5: Central zone lengths λ_z versus cross section for the data and (ECM), (RCM), and (LCM) models.

Figure 6: Central zone rapidity versus cross section for the data and (ECM), (RCM), and (LCM) models.

Figure 7: Rapidity gap distributions showing cross section versus Δy for gaps with $\Delta Q = 0, \pm 1, \pm 2$.

Figure 8: Probability distributions ($P_{\Delta Q = \pm 2}$) displaying probability versus rapidity gap Δy for gaps with $\Delta Q = \pm 2$.

Figure 9: Semi-inclusive V_1 showing $V_1 = \sum_{i=1}^{n-1} |\Delta Q_i|$, the event-to-event average of the sum of the absolute value of all charge exchanges in the event, versus charge multiplicity, n_{ch}, for the data, (RCM), (ECM), and (LCM) models.

Figure 10: Semi-inclusive V_2 showing

$$V_2 = \frac{\sum_{i=1}^{n-1} |\Delta Q_i| \Delta y_i}{\sum_{i=1}^{n-1} \Delta y_i},$$

the gap-weighted average charge exchanges versus charge multiplicity, n_{ch}, for the data, (ECM), (RCM), and (LCM) models.

Figure 11a: Charge asymmetry in rapidity showing $A(y) = \frac{\left(\frac{d\sigma}{dy}\right)_+ - \left(\frac{d\sigma}{dy}\right)_-}{\left(\frac{d\sigma}{dy}\right)_+ + \left(\frac{d\sigma}{dy}\right)_-}$,

the charge asymmetry parameter versus rapidity as measured inclusively.

Figure 11b: Same as fig. 11a for particles produced in the central region only.

Figure 12a: Momentum distributions displaying the cross section versus transverse (P_T) and longitudinal (P_L) momenta measured inclusively in the interaction CMS.

Figure 12b: Same as fig. 12a for fireball products as measured in the fireball rest system.

Figure 13: Angular distributions of fireball products displaying cross section versus cosine of the angle with respect to the beam direction in the fireball system (Θ), for $p < 200$ MeV/c, 200 MeV/c $< p <$ 400 MeV/c, 400 MeV/c $< p <$ 600 MeV/c, and $P >$ 600 MeV/c.

Figure 14: Fireball multiplicities showing cross section versus the charged multiplicity of the central fireballs.

Figure 15: Mass dependence of fireball multiplicity showing average charged multiplicity versus mass of the fireball.

Figure 16: Fireball momentum distributions showing cross section versus momentum of the fireball particles. The solid curve is the result of a fit to the Bose distribution

$$F(p) = \frac{A\,p^2}{e^{E/T}-1}$$

resulting in a temperature $T = 131 \pm 2$ MeV.

TABLE I

DISPERSION OF THE CHARGE TRANSFER

DATA	0.94 ± .03
RCM	1.86
LCM	1.02
ECM*	0.43

* For the ECM model, U = 0 by its nature.

TABLE II

AVERAGE NUMBER OF ZONES

CHARGED MULTIPLICITY	DATA	RCM	LCM	ECM
4	2.60±.02	2.0	2.6	3.0
6	3.15±.02	2.5	3.2	4.0
8	3.68±.03	2.8	3.7	5.0
10	4.06±.05	3.3	4.2	6.0
12	4.51±.08	3.6	4.6	7.0
14	4.76±.16	4.0	4.9	8.0
16	5.53±.33	4.1	5.5	9.0
INCLUSIVE	3.41 ± .02	2.71	3.47	4.64

TABLE III

AVERAGE MULTIPLICITY OF CENTRAL ZONES

CHARGED MULTIPLICITY	DATA	RCM	LCM	ECM
4	2.00±.00	2.0	2.0	2.0
6	2.26±.02	2.3	2.2	2.0
8	2.42±.02	2.5	2.3	2.0
10	2.67±.03	2.8	2.5	2.0
12	2.82±.06	3.0	2.7	2.0
14	3.00±.12	3.2	2.9	2.0
16	3.08±.23	3.4	3.1	2.0
INCLUSIVE	2.54±.02	2.69	2.46	2.00

TABLE IV

AVERAGE CENTRAL ZONE LENGTHS

DATA	.76 ± .01
RCM	.83
LCM	.72
ECM	.52

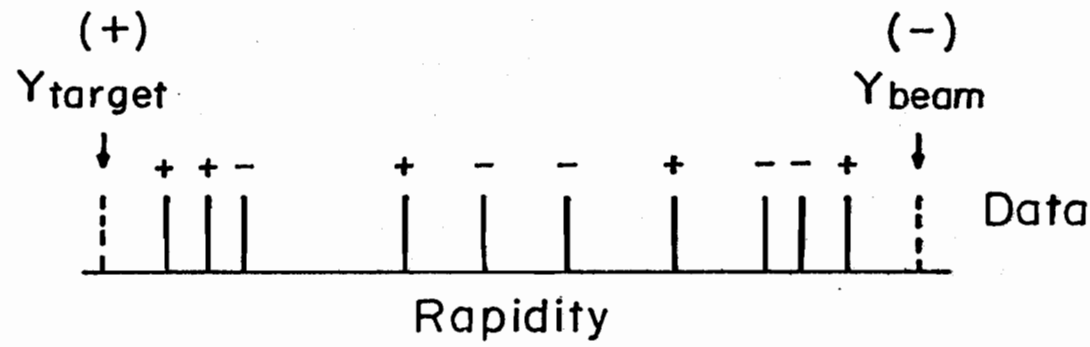
(+)
(−)
Ytarget
Ybeam
+ + −
+ − − + − − +
Data
Rapidity

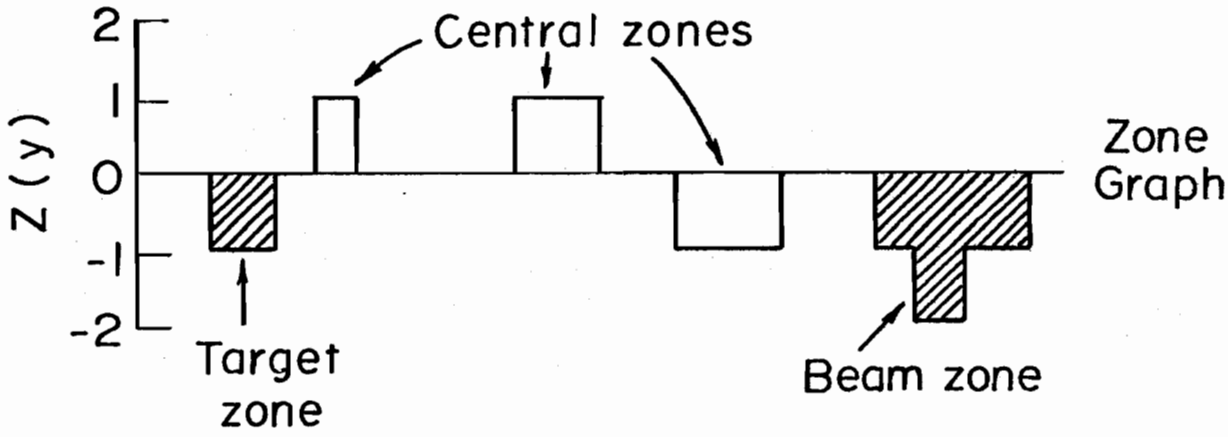
2
1
0
-1
-2
Z(y)
Central zones
Zone
Graph
Target
zone
Beam zone

Figure 1

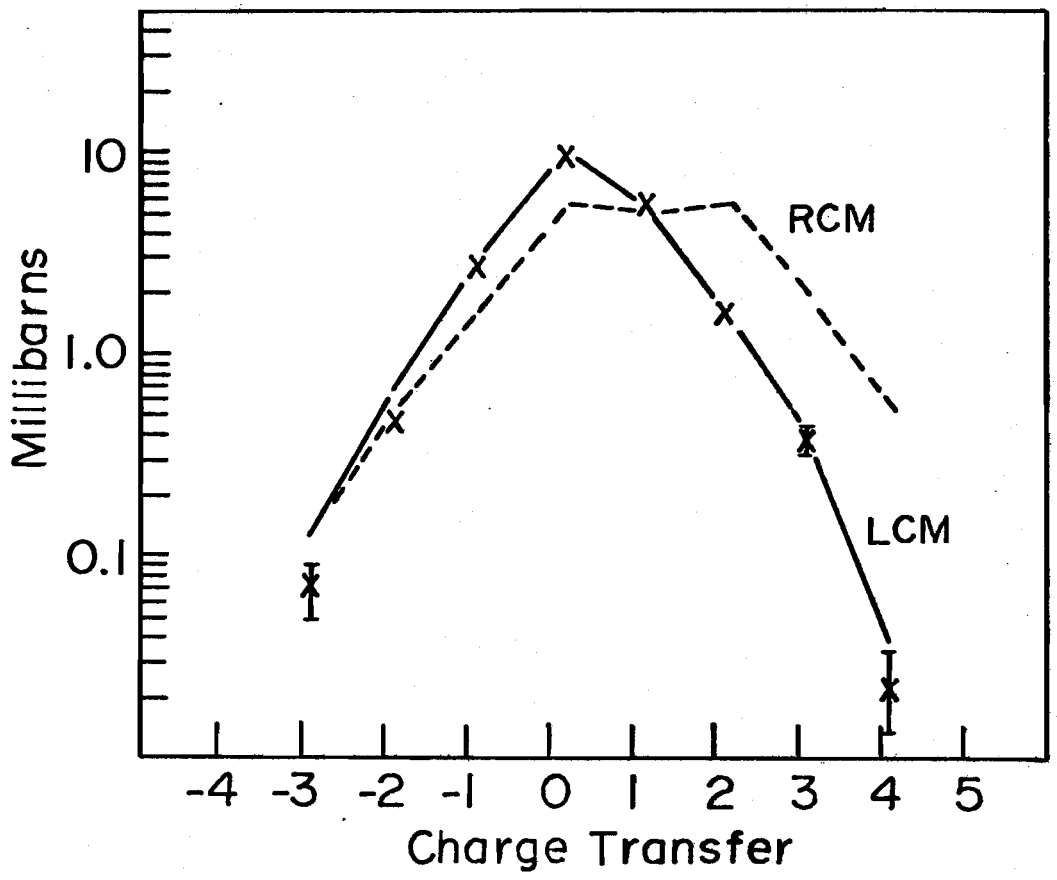

Figure 2

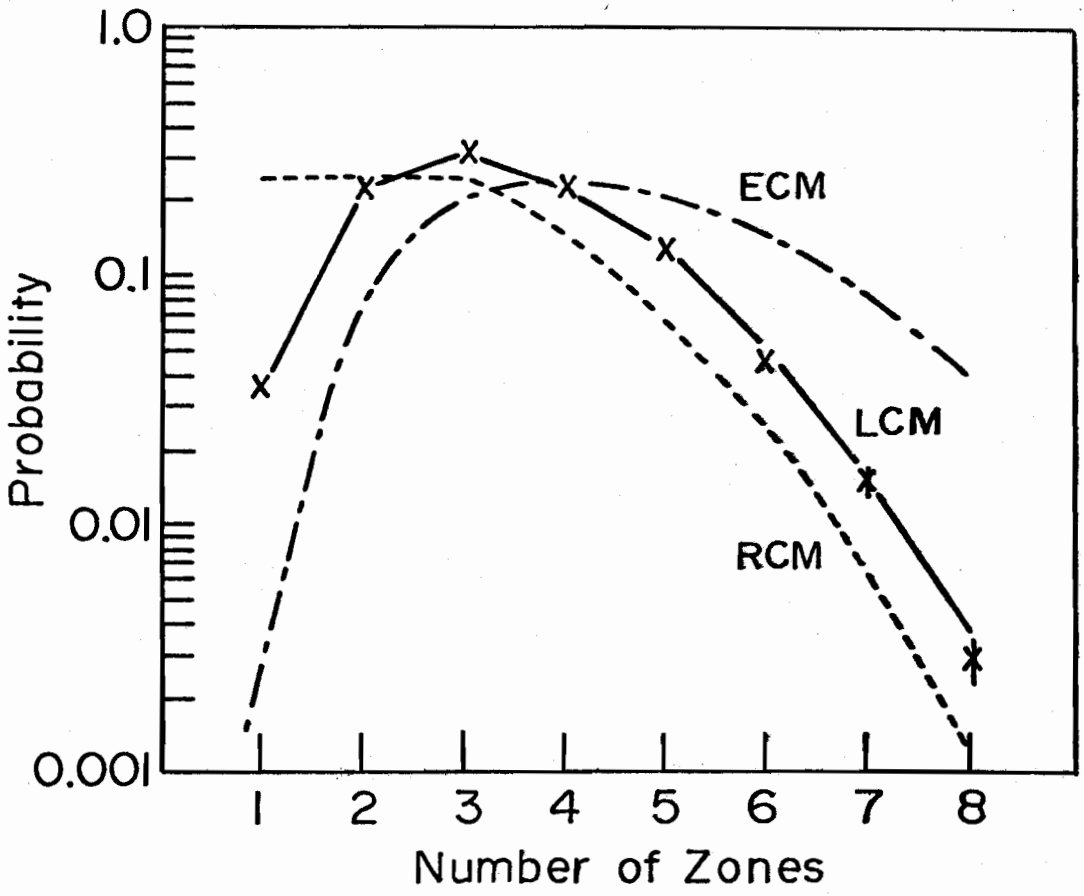
1.0
0.1
0.01
0.001
Probability
ECM
LCM
RCM
1
2
3
4
5
6
7
8
Number of Zones

Figure 3

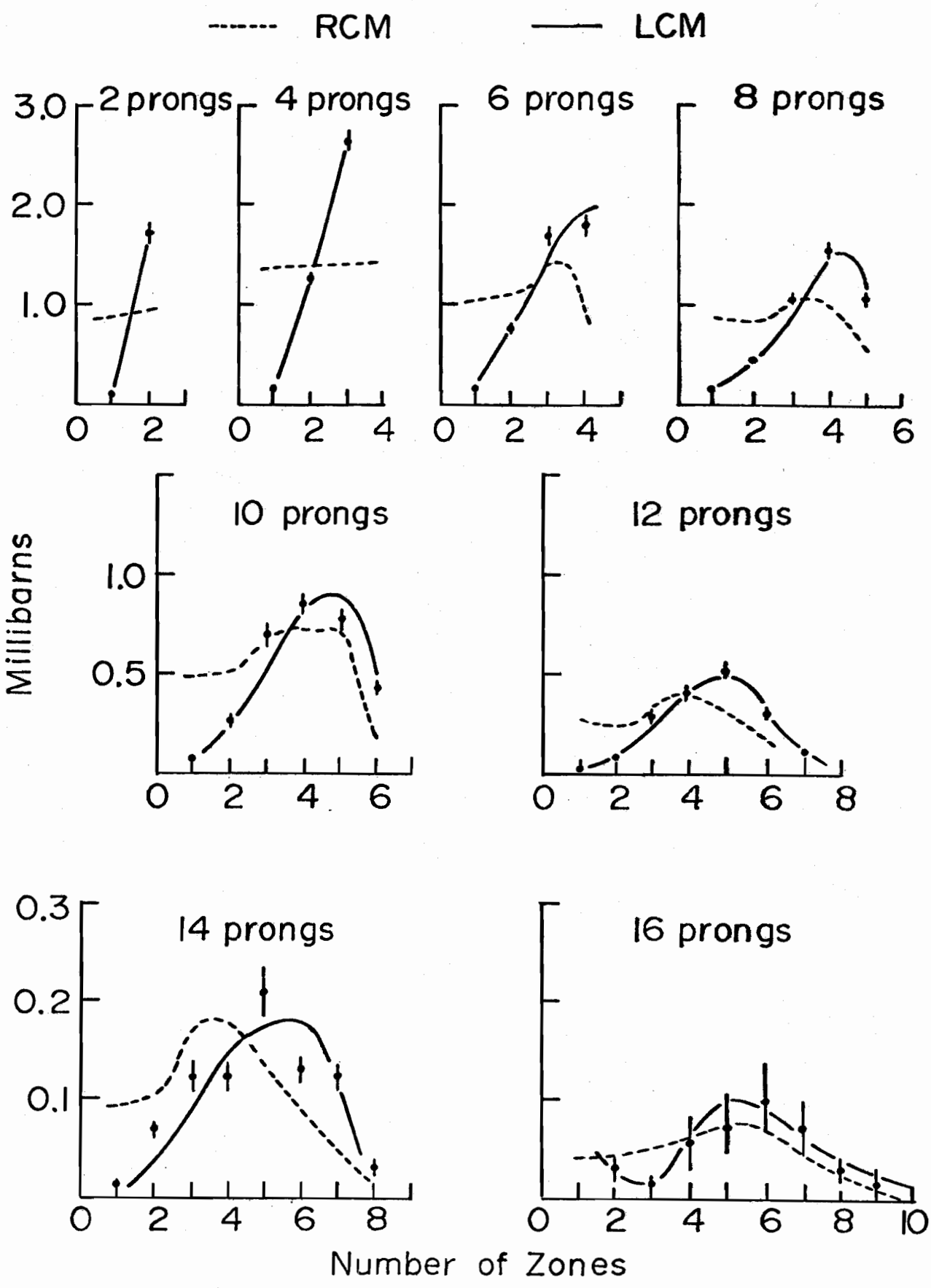
RCM
LCM
2 prongs
4 prongs
6 prongs
8 prongs
10 prongs
12 prongs
14 prongs
16 prongs
Millibarns
Number of Zones

Figure 4

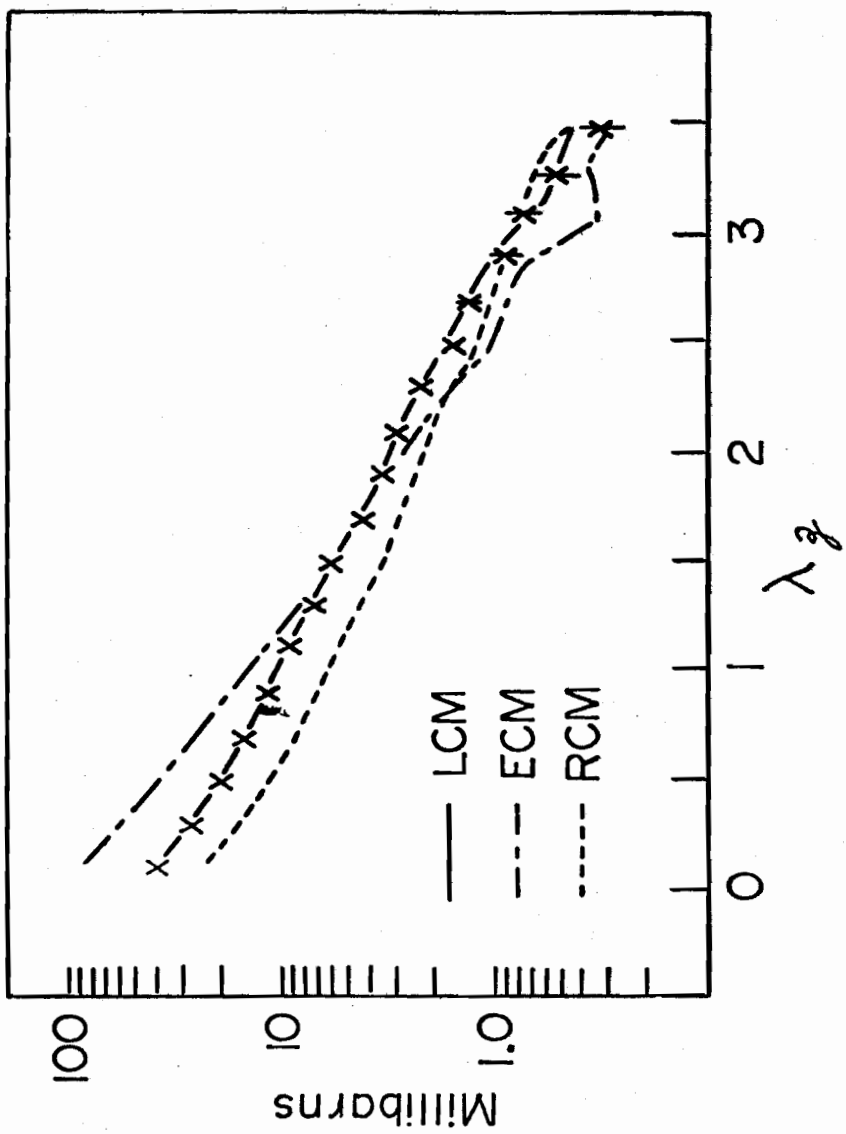

Figure 5

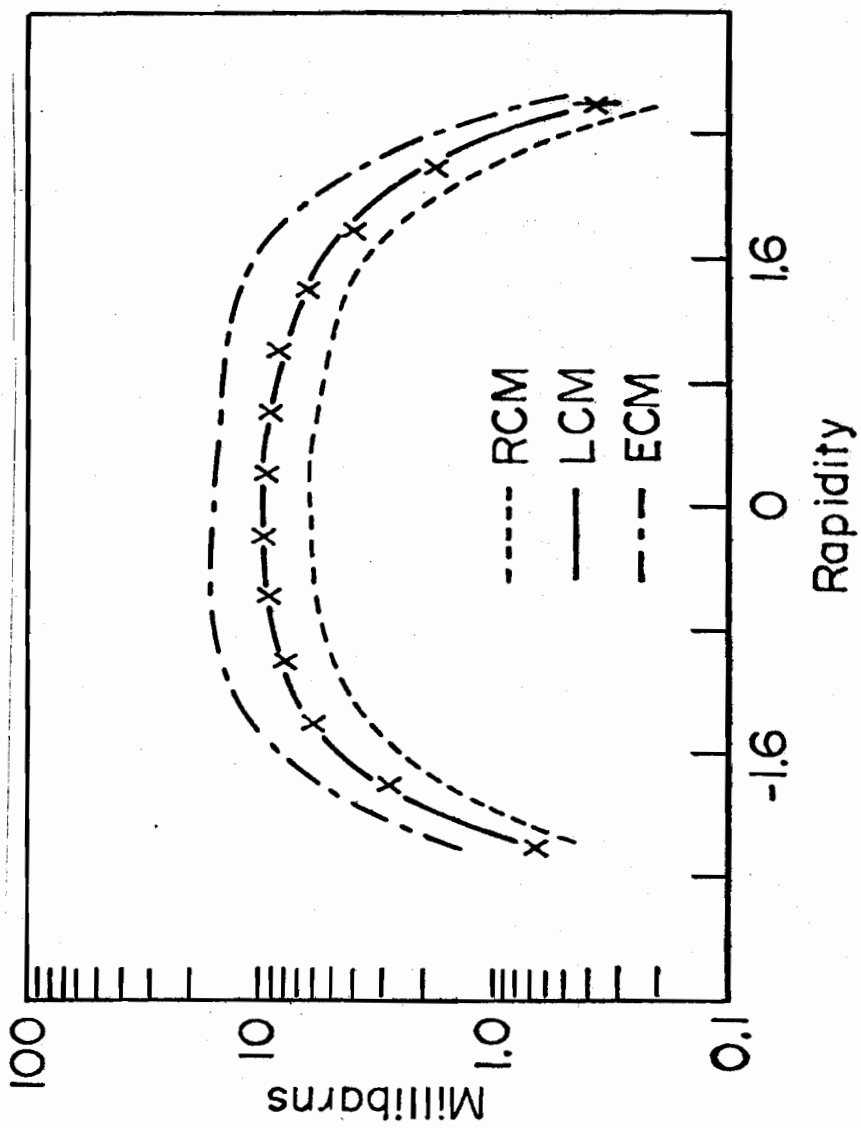

Figure 6

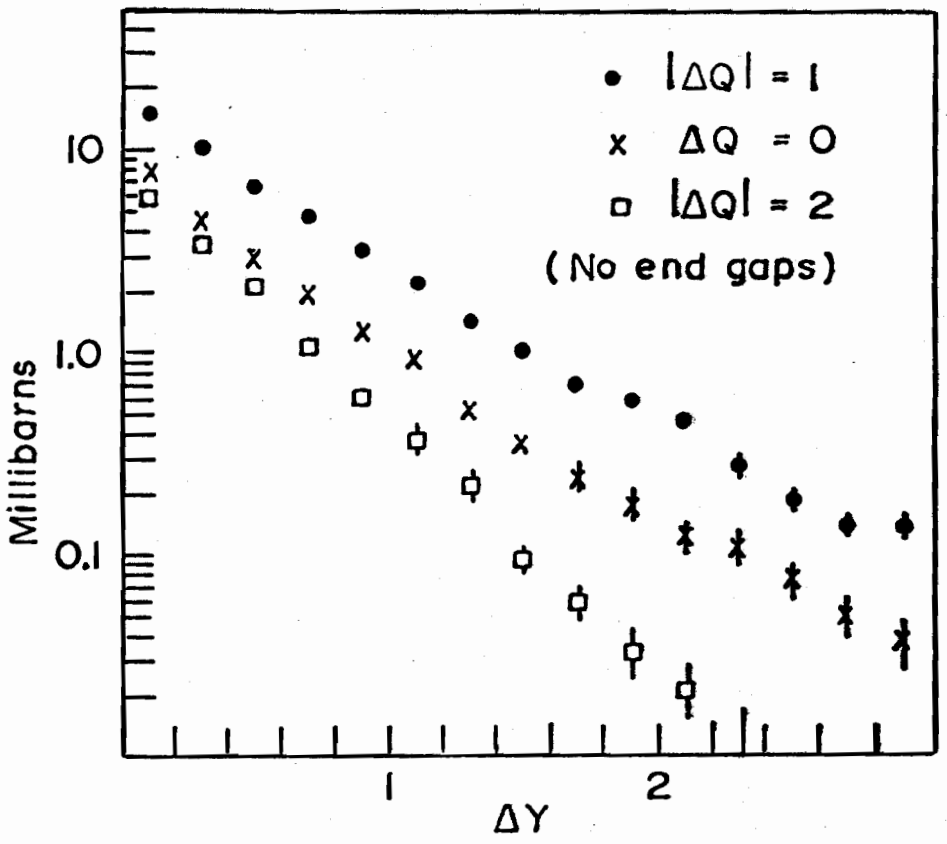

Figure 7

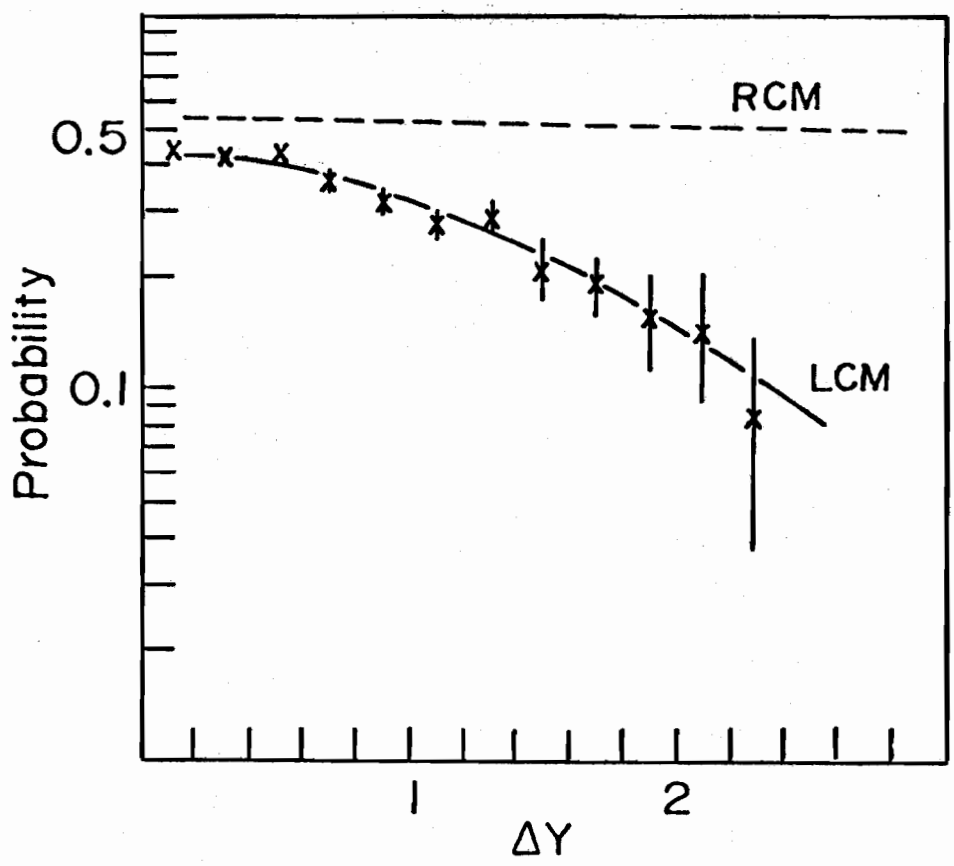

Figure 8

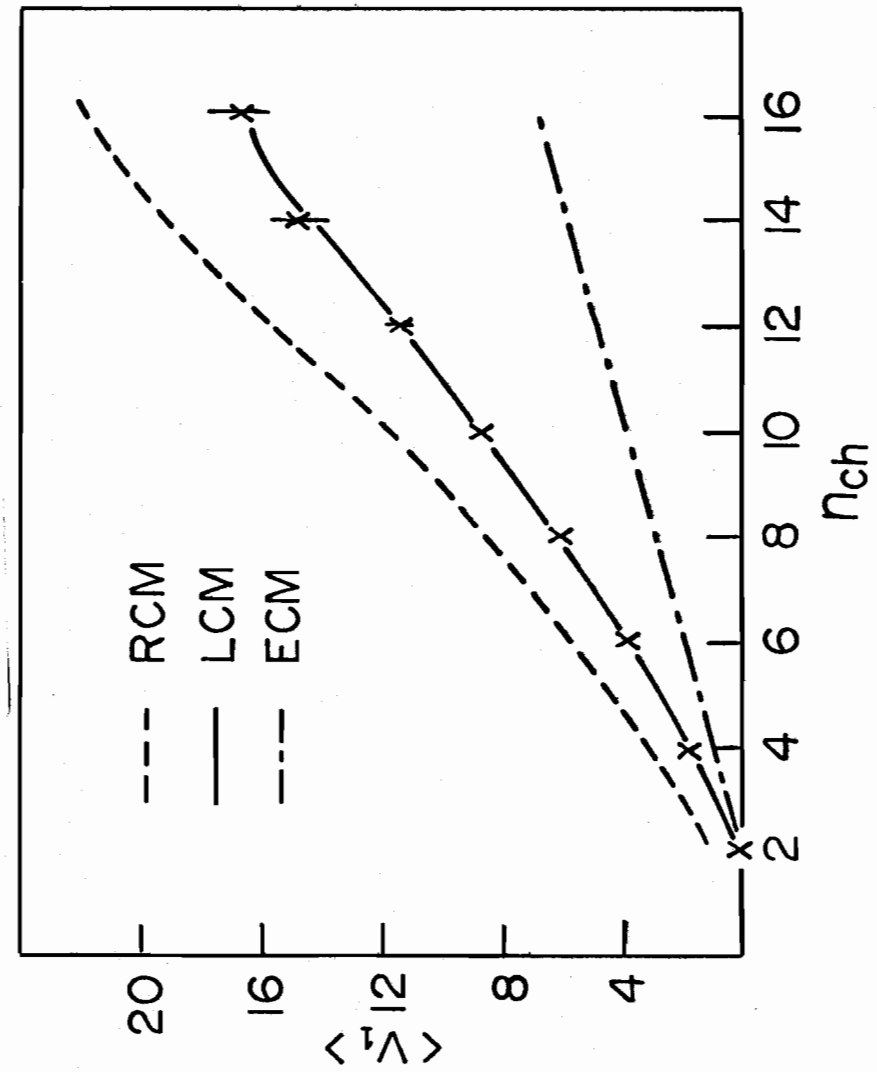

Figure 9

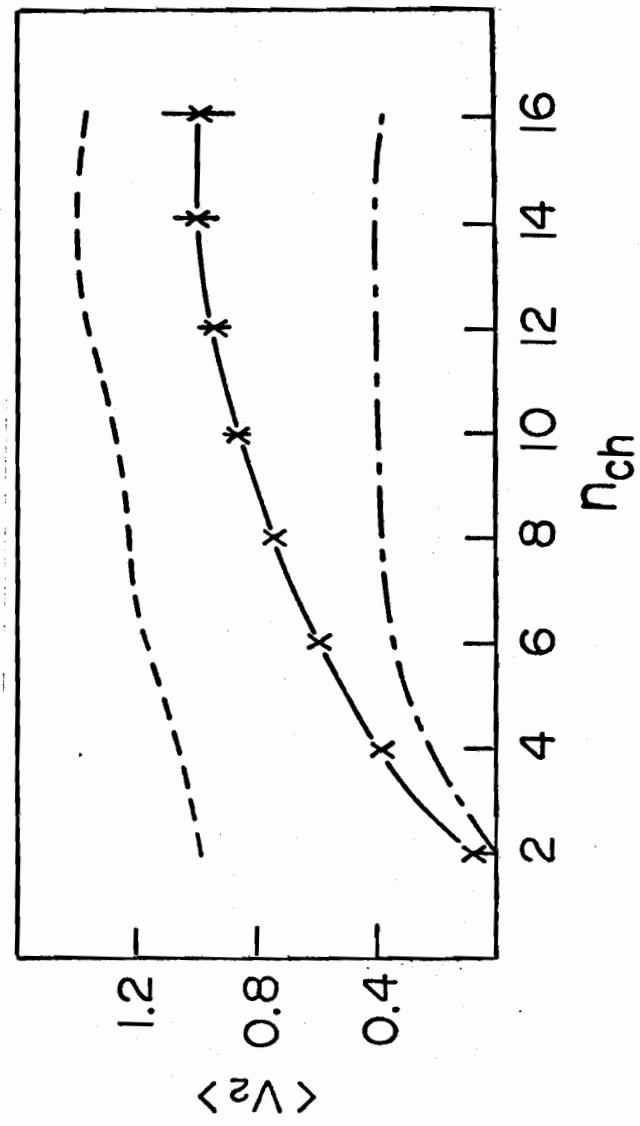

Figure 10

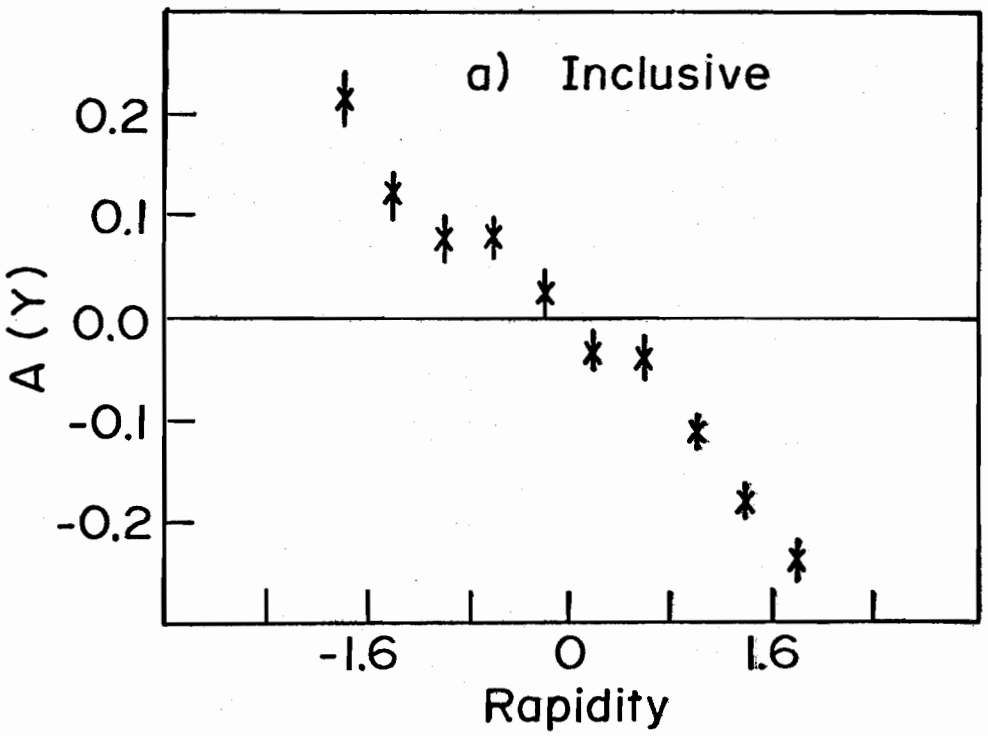
a) Inclusive
0.2
0.1
0.0
-0.1
-0.2
A(Y)
-1.6
0
1.6
Rapidity

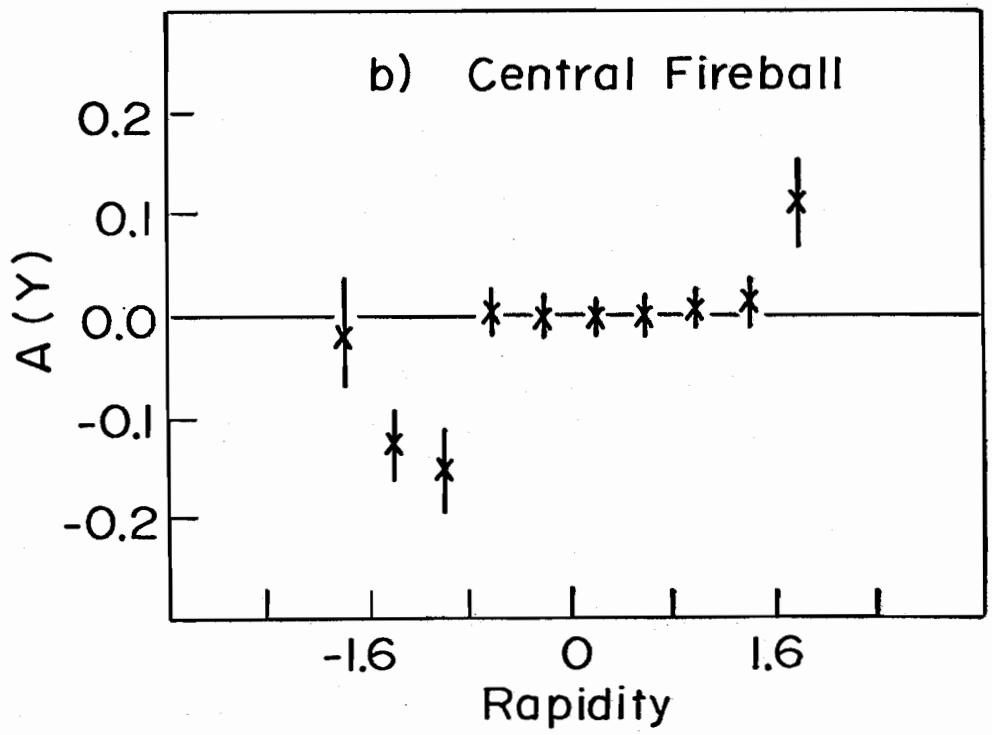
b) Central Fireball
0.2
0.1
0.0
-0.1
-0.2
A(Y)
-1.6
0
1.6
Rapidity

Figure 11

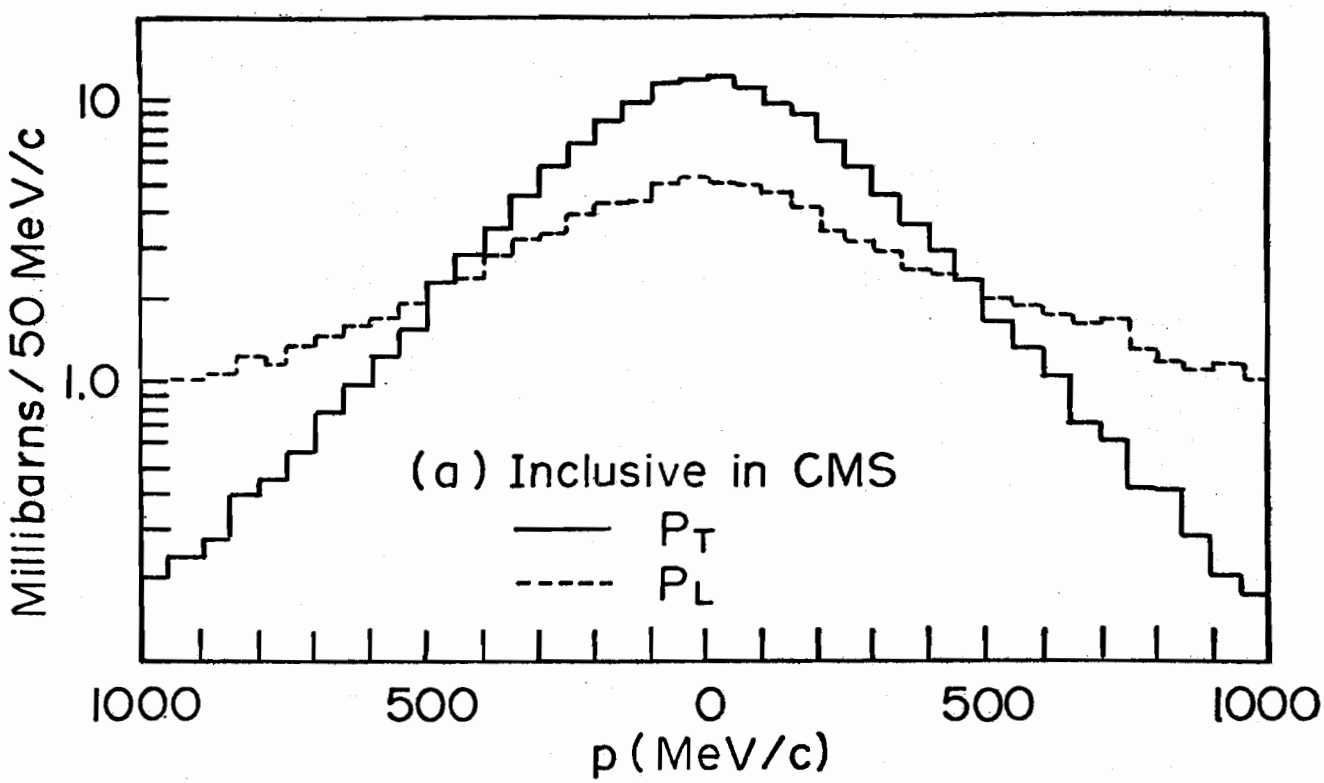
10
1.0
Millibarns/50 MeV/c
(a) Inclusive in CMS
P_T
P_L
1000
500
0
500
1000
p (MeV/c)

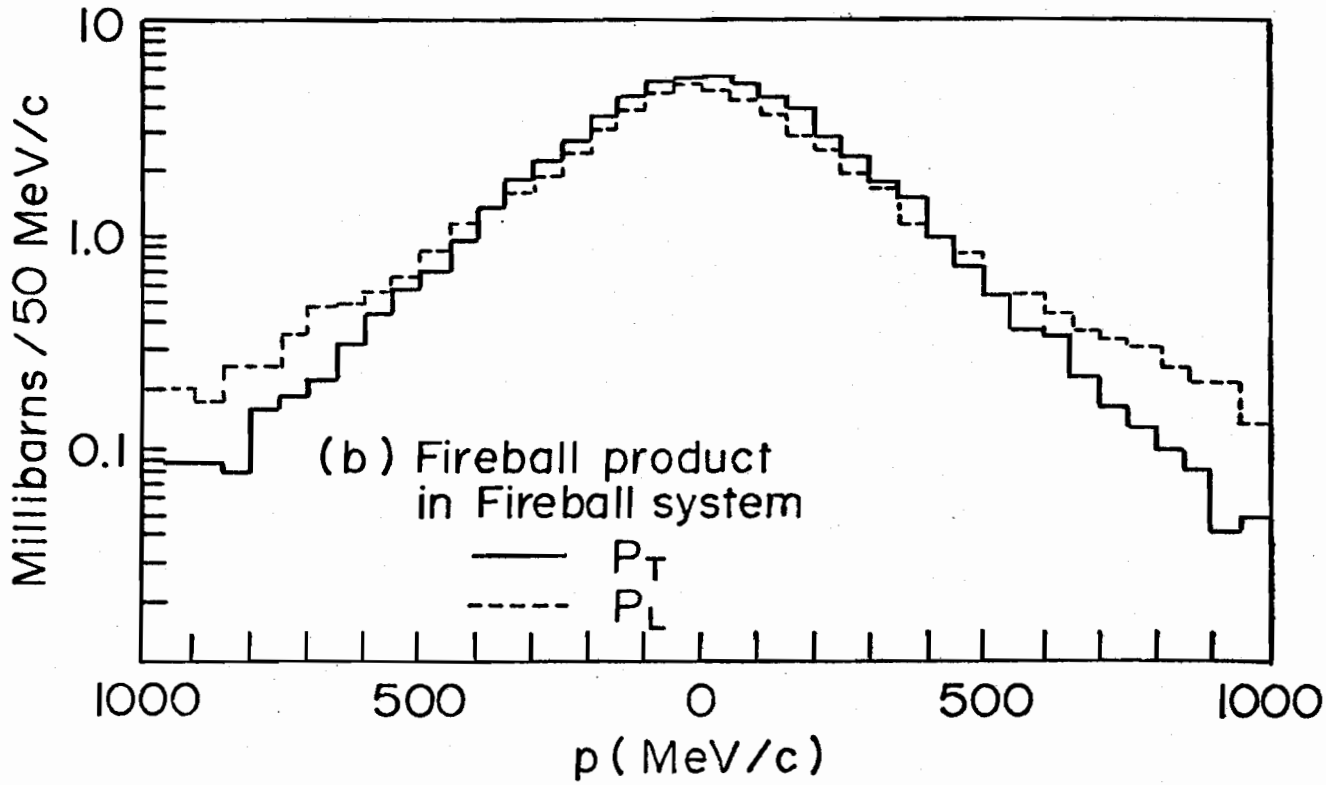
10
1.0
0.1
Millibarns/50 MeV/c
(b) Fireball product
in Fireball system
P_T
P_L
1000
500
0
500
1000
p (MeV/c)

Figure 12

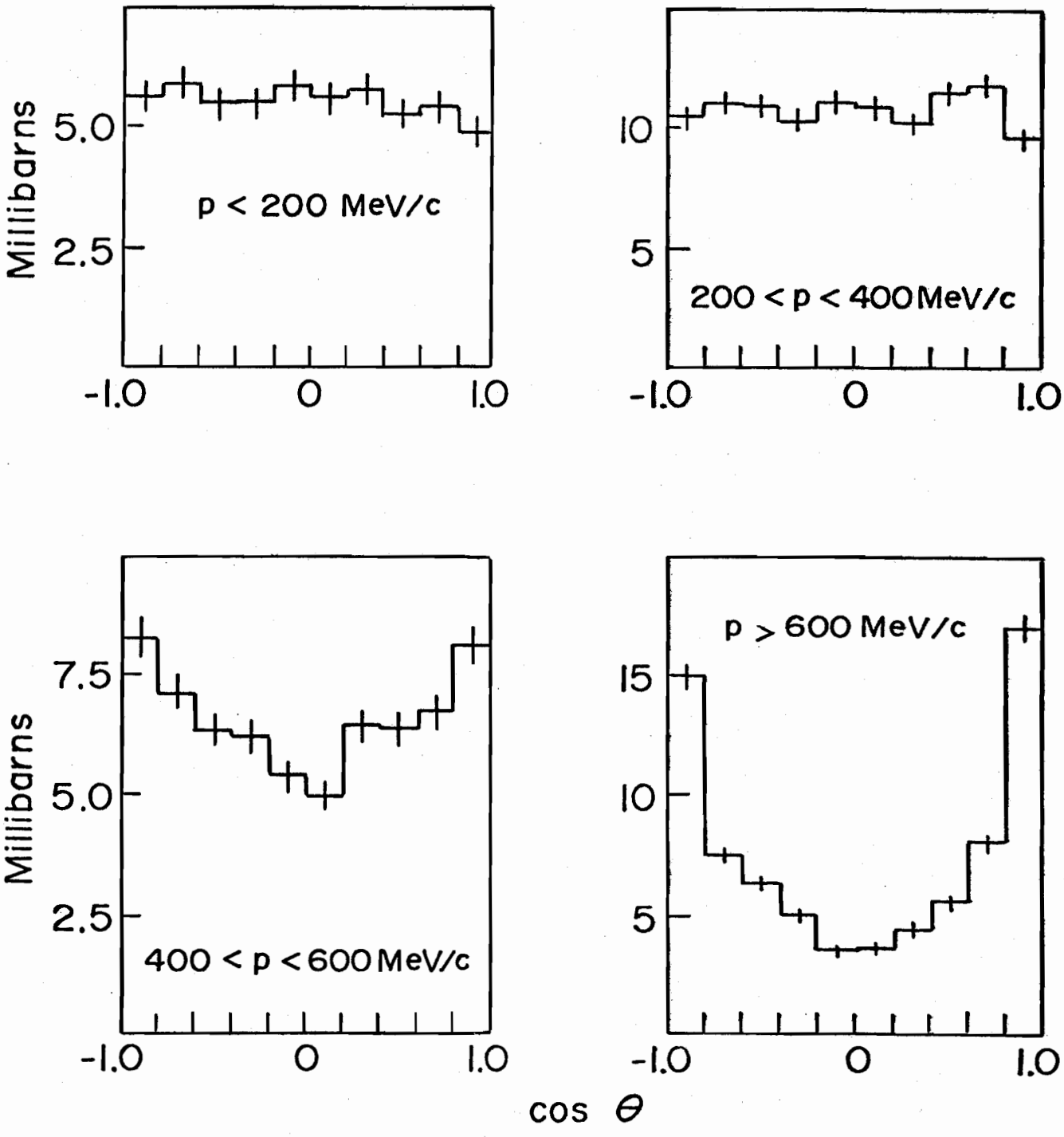
Millibarns
5.0
2.5
p < 200 MeV/c
-1.0
0
1.0
10
5
200 < p < 400 MeV/c
7.5
5.0
2.5
400 < p < 600 MeV/c
p > 600 MeV/c
15
10
5
cos θ

Figure 13

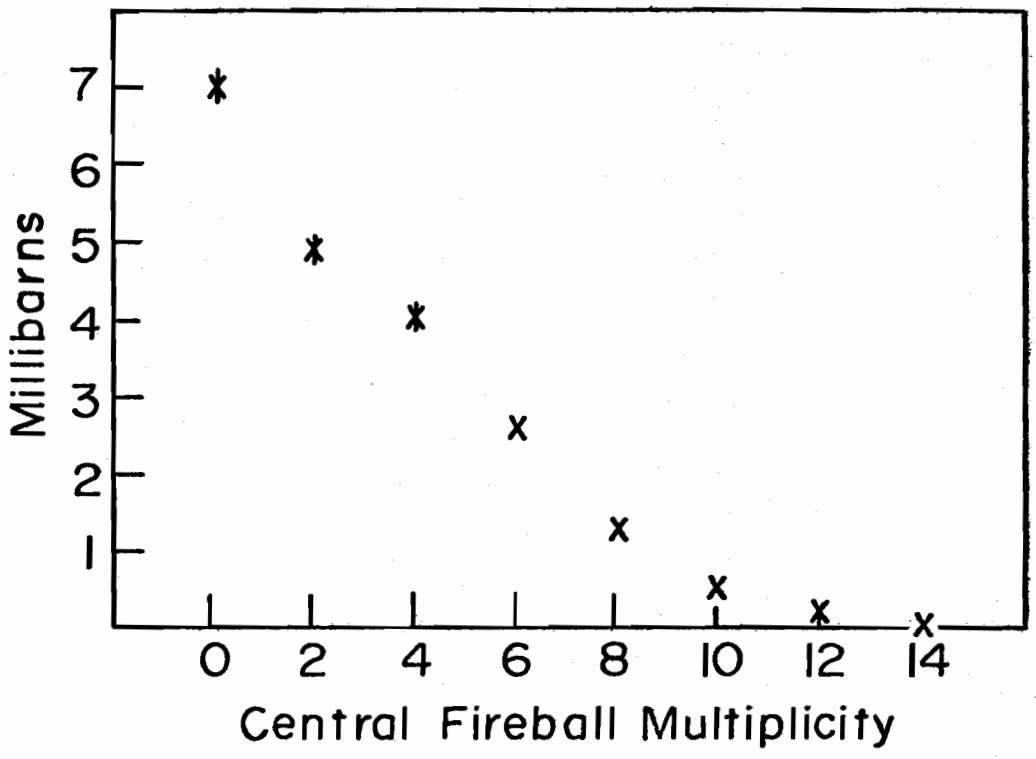
Millibarns
7
6
5
4
3
2
1
0
2
4
6
8
10
12
14
Central Fireball Multiplicity

Figure 14

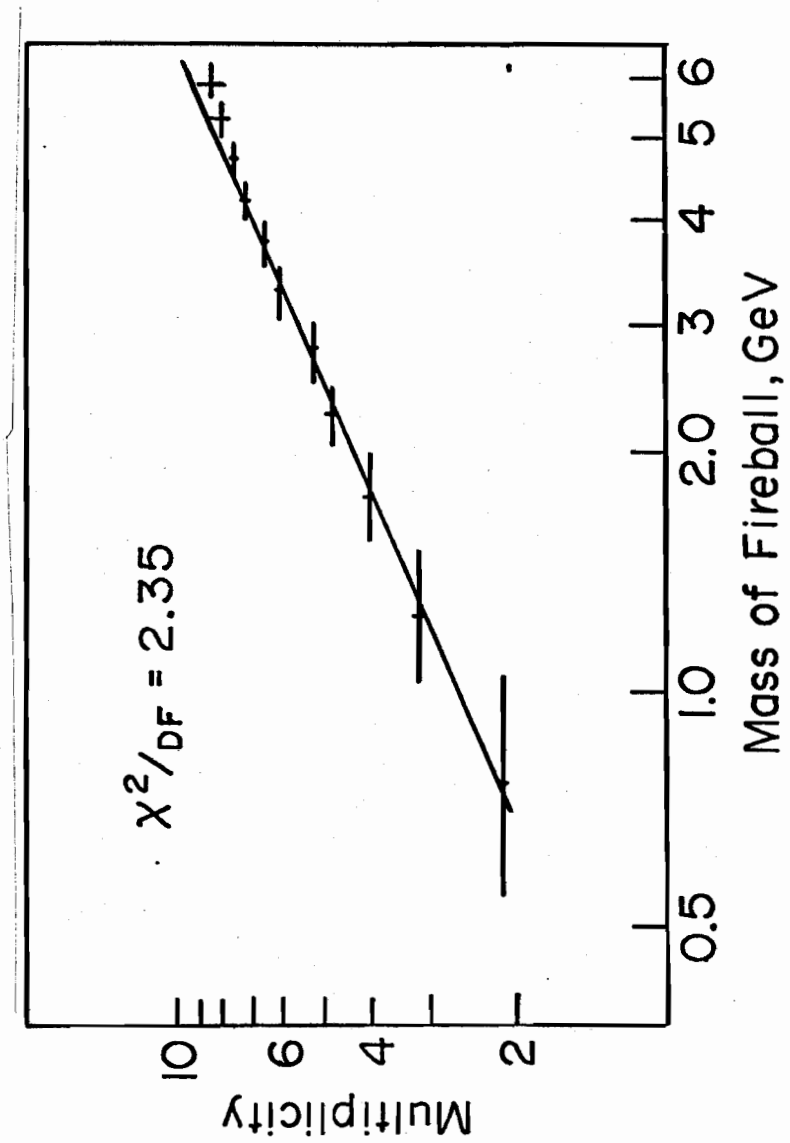
Multiplicity
10
6
4
2
0.5
1.0
2.0
3
4
5
6
Mass of Fireball, GeV
$\chi^2/_{DF} = 2.35$

Figure 15

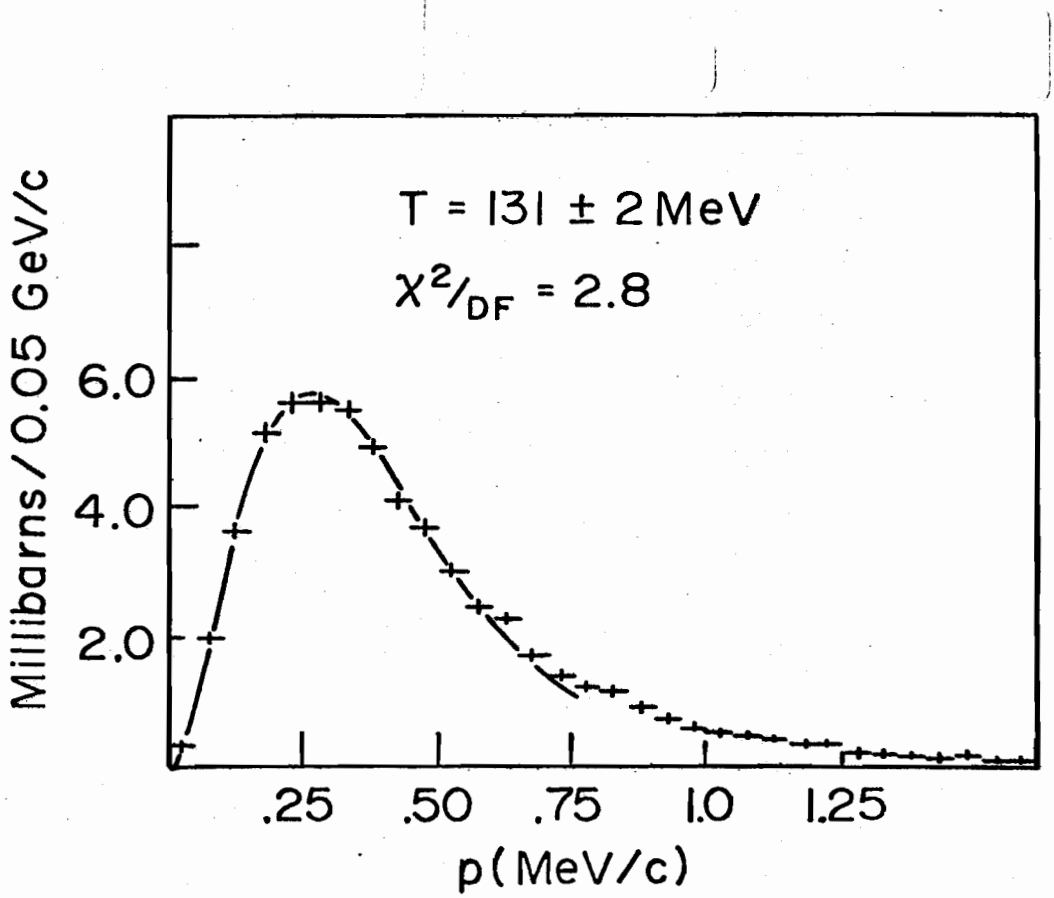
T = 131 ± 2 MeV
$\chi^2/_{DF}$ = 2.8
Millibarns / 0.05 GeV/c
6.0
4.0
2.0
.25
.50
.75
1.0
1.25
p(MeV/c)

Figure 16